Building and Environment 46 (2011) 1834–1842

Contents lists available at ScienceDirect

Building and Environment

journal homepage: www.elsevier.com/locate/buildenv

Application of exceedance probability based on wind kinetic energy to evaluate the pedestrian level wind in dense urban areas

Mahmoud Bady [a,*], Shinsuke Kato [b], Yoshihiro Ishida [b], Hong Huang [b], Takeo Takahashi [b]

[a] Mechanical Engineering Department, Assiut University, Assiut 271516, Egypt
[b] Institute of Industrial Science, The University of Tokyo, 4-6-1 Komaba, Meguro-ku, Tokyo 153-8505, Japan

ARTICLE INFO

Article history:
Received 30 September 2010
Received in revised form
9 March 2011
Accepted 10 March 2011

Keywords:
Exceedance probability
Wind kinetic energy
Urban ventilation
Wind environment
Built-up area

ABSTRACT

In the present study, assessment of wind environment within the pedestrian level domains of highly populated areas is carried out. Three typical models of a dense urban area are considered and numerically simulated in order to examine the effects of the geometry of such models on wind flow characteristics within the pedestrian domain of a street canyon located within this area. The calculated flow fields are employed to estimate the exceedance probabilities within the study domain using a new approach: average wind kinetic energy. The study is applied to Tokyo, Japan; based on its mean wind velocity data. The results demonstrate that the exceedance probability analysis of the pedestrian wind environment could be a valuable tool for assessing urban areas. Also, the calculated probabilities demonstrate substantial dependence on both the geometry of building arrays and the wind conditions of the considered domain.

1. Introduction

High-density building arrays can affect wind flow characteristics at pedestrian level, which in turn affects the acceptability of the wind conditions for pedestrian use. Consequently, demonstration of a satisfactory wind environment at the pedestrian level of such areas is required to ensure a reasonable level of comfort for inhabitants. From this perspective, the present research sheds light on how to analyze pedestrian wind environments within dense urban areas through the application of exceedance probability to assess the wind conditions of such areas.

Many researchers have studied wind conditions in urban areas and used the exceedance probability analysis to assess the safety and regular wind discomfort in such areas. Most of these studies focused on pedestrian level winds. Melbourne [7] studied assessment of prospective environmental wind conditions regarding a proposed building development in Australia. He described a method for predicting the probability of occurrence of a given wind speed at a particular location. Murakami [10] constructed criteria for assessing wind conditions on the basis of wind speed and survey of residents' opinions over a long period of time. They used the exceedance probability analysis based on the Weibull distribution to describe their criteria, and they applied such criteria in evaluating the wind conditions in a typical city center area. Ohba et al. [12] carried out actual field measurements in order to study wind conditions at ground level around a redevelopment area in Tokyo. They used 17 measurement points to assess whether the wind conditions were acceptable or not based on three published criteria: Murakami [10], Melbourne [6] and Isyumov N and Davenport AG [7]. Their study results demonstrate that Murakami's criterion is midway between those of Melbourne and Davenport. Similar to the previous study, Ratcliff and Peterka [14] carried out wind tunnel measurements of pedestrian wind speeds for nine building projects to evaluate five different criteria using exceedance probability. Visser and Cleijne [18] carried out wind tunnel experiments and full scale measurements to predict the wind climate around two buildings through the application of the exceedance probability approach. Murakami [9] conducted observations of wind flow at ground level over a period of 2 years around a high-rise apartment building in a built-up area in Tokyo. They derived approximation of the exceedance probability for mean wind velocity and gust wind velocity at ground level by the Weibull distribution and they concluded that the approximation by the Weibull distribution becomes more accurate if the wind data for each wind direction is approximated separately and then those distributions are summed up. As an overview of previous studies, Stathopoulos [16] addressed experimental and computational evaluations of the wind on people in an urban environment and focused on the development of human outdoor comfort criteria by considering a wide range of parameters, including wind speed, air temperature, relative humidity, solar

* Correspondence author. Tel.: +20 19 1844514; fax: +20 88 233 2553.
E-mail address: mbady@aun.edu.eg (M. Bady).

0360-1323/$ – see front matter © 2011 Elsevier Ltd. All rights reserved.
doi:10.1016/j.buildenv.2011.03.003

radiation, air quality, human activity, clothing level, age and the like. He described an approach for establishing an overall comfort index taking into account, in addition to wind speed, the temperature and relative humidity in the urban area under consideration. Blocken et al. [3] carried out numerical simulations in order to assess the wind climate in the passages of three high-rise residential buildings in the city of Antwerp, Belgium. They found that the wind climate is highly unacceptable and accordingly, the authors have designed and analyzed an automatic control system to modify the wind climate in the passages. The exceedance probability was used not only for the assessment of wind climate but also -and especially- for the analysis of the automatic control system. In another study by Blocken and Carmeliet [2], the exceedance probability was employed to assess the wind comfort at outdoor platforms for different design modifications of a high-rise apartment building. Based on their study, structural remedial measures for the considered building succeeded to bring the discomfort probability estimates down to acceptable levels. More recently, Bady et al. [1] have applied the exceedance probability to evaluate the wind ventilation effectiveness in dense urban areas based on a new approach; air exchange rate.

In the present study, the exceedance probability is introduced via another new approach: wind kinetic energy (*KE*), as a reflection of human comfort. The new approach is introduced based on the fact that the wind kinetic energy is proportional to the wind velocity. Moreover, the previous work demonstrated that the calculation of exceedance probability was carried out based on the velocity at one point located within the study domain, while it is very important to consider the entire volume of the pedestrian domain. The present paper takes this issue into account.

In order to carry out this study, firstly, computational fluid dynamics (CFD) simulations were performed in order to calculate the flow fields within the wind environment. An extensive amount of wind tunnel experiments were carried out in the same time to measure wind velocities and pollutant concentrations along the sides of the street domain for different geometries and different wind directions [1]. Then, the calculated flow fields were evaluated by comparing numerical and experimental data for wind velocity and gas concentrations within the street domain. Secondly, the calculated flow fields were employed to estimate wind kinetic energies within the pedestrian domain of the street.

2. Model description

Three typical models of a densely built-up area are illustrated in Fig. 1, and the geometry of the central part of model (I) is shown in Fig. 2. In Fig. 1, the white blocks express detached houses, while the grey area represents traffic roads and voids between adjacent buildings. The study domain (in all of these models) is the pedestrian volume located along a street surrounded by type-A and type-B blocks (shown in Fig. 2) and a fence of 1.5 m height around these blocks. The study domain has the same dimensions as the street (40 m × 4 m) and extends to a height of 5.5 m.

Models (I), (II), and (III) have the same building arrangements and dimensions, but they differ in the geometry of the central part which surrounds the street (marked with black dashed lines). In model (I), the central part consists of eight type-A and two type-B blocks. Narrow gaps of 1 m width exist between the types-A buildings, and also between the type-B buildings. In model (II), the central part forms a solid U-shape. With respect to model (III), the street buildings are the same as those of model (I), while the outer blocks which surround them form a solid U-shape.

Many factors were born in mind during the design of these three building patterns. First, these models suit the nature of existing small-lot residential areas in Japan, as demonstrated in [5]. In the study in Ref. [5]; Katsumata stated that the small-lot residential areas are widespread developed in suburbs of metropolitan area in Japan while the rapid economic growth era, 1960–70s is matured. Also, the author stated that the environmental conditions such as daylight and wind ventilation rate became worse due to the construction of high-rise houses, which were built in order to increase the available living area. Second, the three models were nominated to examine the optimum design for densely inhabited areas, which will induce more wind inside urban domains and will improve their air quality. Third, model (II) represents an unfavorable choice for dense urban areas, due to the blocking effect of its geometry in some wind directions. The U-shape of the central part of such model decelerates the wind motion and hence traps pollutants within the pedestrian domain of the street. Fourth, model (I) represents a spatially uniform-building array. Fifth, model (III) exhibits a combination between models (I) and (II), and as a result, it is expected to demonstrate behavior between these two models.

3. Methodology

As previously mentioned, the exceedance probability is introduced in this paper via wind kinetic energy, as a reflection of comfort. This approach is introduced based on the fact that wind kinetic energy is proportional to the wind velocity.

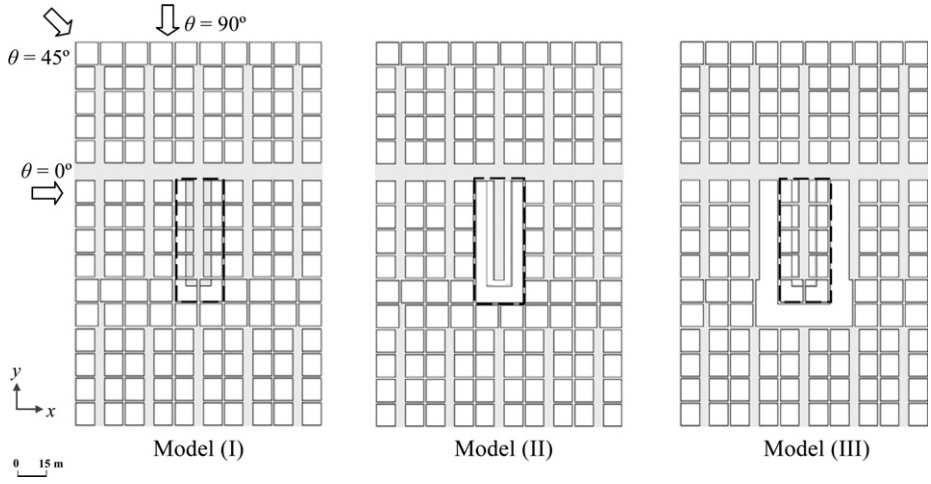

Fig. 1. Simplified diagrams for the three typical models of a dense urban area.

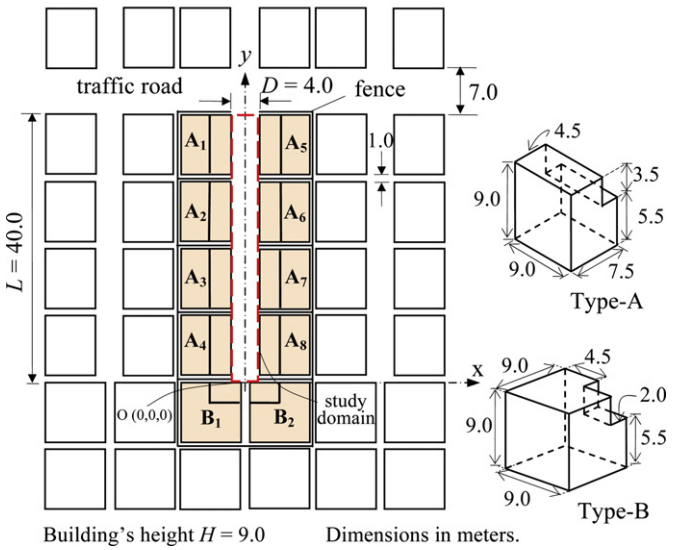

Fig. 2. Street characteristics in the case of model (I).

3.1. Wind kinetic energy

The average wind kinetic energy is a measure of airing around enclosed environments, since it represents the wind potential for comfort. The total kinetic energy in a cell is the summation of mean and turbulent kinetic energies in such cell. Then, the average kinetic energy within a domain is calculated according to the equation:

$$KE = \frac{1}{V_p}\sum\left\{\frac{1}{2}\left(u^2+v^2+w^2\right)+k\right\}\Delta v \tag{1}$$

where:

KE is the average wind kinetic energy (m^2/s^2).

V_p is the domain volume (m^3).

u, v, and w are the ensemble-averaged velocity components in each cell (m/s).

k is the ensemble-averaged turbulent kinetic energy (m^2/s^2).

Δv is the cell volume (m^3).

The kinetic energy is also calculated using CFD simulations and it is used to evaluate the total exceedance probability for different wind directions.

3.2. Exceedance probability

The exceedance probability is a measure of the ventilation performance of the applied wind within a certain urban domain. It is described by the Weibull distribution which, for any azimuth direction a_n (i.e. a_o = N, a_1 = NNE… a_{15} = NNW), is expressed as [10,12]:

$$P(V_{exceed} > V_g) = A(a_n) \times \exp\left\{-\left(\frac{V_g}{C(a_n)}\right)^{K(a_n)}\right\} \tag{2}$$

In this equation; $P(V_{exceed} > V_g)$ is the probability of exceeding a reference velocity V_g (shown in Fig. 3), $A(a_n)$ is the relative frequency of occurrence, and $C(a_n)$ and $K(a_n)$ are Weibull parameters for each wind direction.

The wind velocity is proportional to the square root of its kinetic energy, so:

$$V \alpha \sqrt{KE} \tag{3}$$

Equation (2) is used to estimate the exceedance probability for the considered reference velocity. In order to calculate the probability for another velocity, the following procedure is applied: a reference velocity referred to as V_{g1}, as illustrated in Fig. 3, is introduced. For such velocity, the wind kinetic energy within the study domain is calculated through CFD simulations to be KE_{g1}. The velocity V_g represents any reference velocity at the same height and the calculated wind kinetic energy at such velocity is KE_g. Since the wind velocity is proportional to the wind kinetic energy, then:

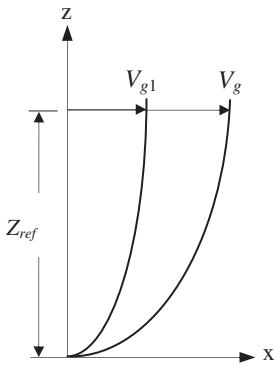

Fig. 3. Definition of V_g and V_{g1}.

$$V_g = \sqrt{\frac{KE_g}{KE_{g_1}}}V_{g1} \tag{4}$$

Substituting Equation (4) into Equation (2), gives:

$$P(V_{exceed} > V_g) = A(a_n) \times \exp\left\{-\left(\frac{\sqrt{KE_g}}{\sqrt{KE_{g1}} \times C(a_n)} V_{g1}\right)^{K(a_n)}\right\} \tag{5}$$

Rearranging the above equation to get:

$$P(V_{exceed} > V_g) = A(a_n) \times \exp\left\{-\left(\frac{\sqrt{KE_g}}{\sqrt{KE_{g1}} \times C(a_n)} V_{g1}\right)^{K(a_n)}\right\} \tag{6}$$

So, the exceedance probability based on wind kinetic energy for any wind direction a_n is:

$$P(V_{exceed} > V_g.a_n) = A(a_n) \times \exp\left\{-\left(\frac{\sqrt{KE_g}}{\sqrt{KE_{g1}} \times C(a_n)} V_{g1}\right)^{K(a_n)}\right\} \tag{7}$$

In order to calculate the total exceedance probability for all directions, integration of Equation (7) from 0° to 360° is required. It is an easy task if the integration is done manually using a coarse sector of 22.5°. In this case, there will be sixteen wind directions (i.e. i = 0, 1… 15) and the final equation becomes:

$$P(V_{exceed} > V_g \cdot a_n) = \sum_{n=0}^{15} A(a_n) \times \exp\left\{-\left(\frac{\sqrt{KE_g}}{\sqrt{KE_{g1}} \times C(a_n)} V_{g1}\right)^{K(a_n)}\right\} \tag{8}$$

Fig. 4 illustrates the procedure for calculating the exceedance probability. For each one of the 16 directions of the building array

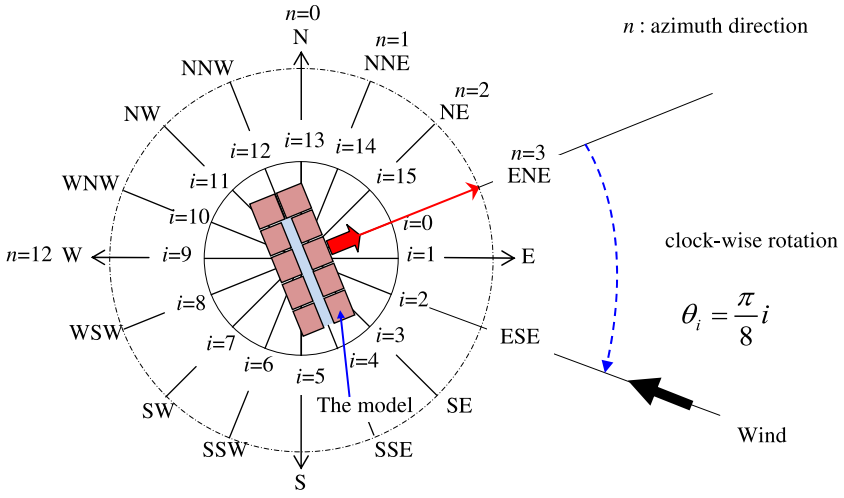

Fig. 4. Explanation of the method for calculating the exceedance probability.

($i = 0$–15), there are sixteen wind directions ($n = 0$–15). This means that in order to estimate the total exceedance probability in all wind directions, 256 cases must be dealt with for every building model. In Fig. 4, the case of an array direction of ENE is illustrated as an example. In such case, the array is set at ENE direction while the incident wind direction is varied from N ($i = 13$) to NNW ($i = 12$) in a clockwise rotation with steps of 22.5°.

In order to carry out the present study, Tokyo was selected to conduct the exceedance probability calculations on. Graphical representations of the parameter $A(a_n)$ for Tokyo is given in Fig. 5. The Weibull parameters was estimated through the regression of the data of mean wind velocity which was measured every 3 h for a period of 10 years starting from 1995 to 2004, and averaged over 10 min. Values of the Weibull parameters for the sixteen azimuth directions in Tokyo are given in Table 1 (see Ref. [19]).

3.3. Numerical simulations

Numerical simulations were carried out through the CFD code STAR-CD, based on a finite-volume discretization method. Steady state analysis was adopted and the Monotone Advection and Reconstruction Scheme MARS [15] was applied to the convective term, and the central difference scheme was used for the diffusion terms. The pressure/velocity linkage is solved via the SIMPLE algorithm [13].

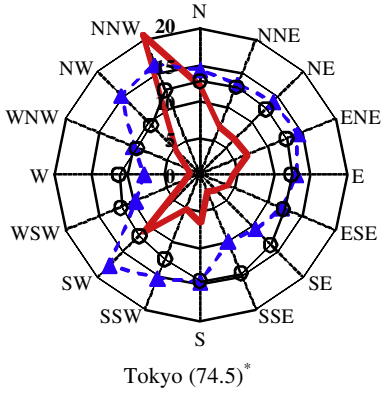

Fig. 5. Wind roses of Tokyo estimated based on mean wind velocity (averaged over 10 minutes) [14]. —: A_n(%), ▲: C_n×4 (m/s), ○: K_n×5(-). (* The numbers in brackets refer to the observation height in meters.).

Since many real flows are anisotropic and the standard k-ε model equations don't account for the anisotropy, a non-linear version of the k-ε model was preferred to simulate the turbulence effects. In this study, the cubic high Reynolds number k-ε model [15] was used because this model caters for the above defect by adopting non-linear relationship between Reynolds's stresses and the rate of strain.

In expectation of greater simulation accuracy, a structured grid system was used to simulate the building arrays. Fine meshes were applied near the walls and around the buildings, and coarse ones were used far from them. In addition, as the passages between street buildings are a very important aspect for the simulation results, very fine meshes were used across the width of each passage, as mentioned by [4]. This arrangement was considered to ensure a proper resolution of the boundary layers and of the air flow in the study domain. Fig. 6 shows a schematic of the grid system for the building array of model (I) together with the grid characteristics of the study domain and the passages.

At the inflow boundary, a constant flux layer was assumed for the turbulent energy k, and turbulent intensity was assumed to be 10% of the inflow wind velocity at a representative height (z_o) of 74.6 m. The turbulent kinetic energy was calculated as given by Equation (9), while the turbulent dissipation rate was calculated according to Equation (10), which arises from the assumption of local equilibrium $P_k \cong \varepsilon$ (P_k: production term for k equation) [8,11,17].

$$k \cong 1.5\,(u_o \times I)^2 \tag{9}$$

$$\varepsilon \cong C_\mu^{1/2} \times k \times \frac{\partial u}{\partial z} \tag{10}$$

where k is the turbulent kinetic energy (m^2/s^2), u_o is the reference wind velocity (m/s), I is the turbulent intensity of the applied flow, u is the wind velocity (m/s), ε is the dissipation rate and C_μ is a constant.

The sides and the top of the computational domain are modeled as slip walls (zero normal velocity and zero normal gradients of all variables). The generalized logarithmic law with the parameter $E = 9$ (m) was applied to the building walls and ground surface as smooth walls. Table 2 summarizes the parameters used in the simulations together with the applied boundary conditions.

Dimensions of the wind environment domain around the building arrays were not fixed. It was varied according to the applied wind direction. For example; when the wind direction was normal to the street (i.e. $\theta = 0°$) the domain dimensions were

Table 1
Weibull parameters for the sixteen azimuth directions in Tokyo (See Ref. [19]).

Parameter	NNE	NE	ENE	E	ESE	SE	SSE	S	SSW	SW	WSW	W	WNW	NW	NNW	N
$A(a_n)$	7.0%	6.7%	7.0%	4.6%	3.9%	2.9%	2.3%	6.6%	5%	11%	2.4%	1.5%	1.7%	4.8%	20.6%	12%
$C(a_n)$	3.34	3.52	3.6	3.28	3.02	2.64	2.48	3.67	3.85	4.39	2.39	1.92	2.48	3.82	4.06	3.58
$K(a_n)$	2.61	2.53	2.55	2.50	2.46	2.71	2.92	2.91	2.50	2.37	2.35	2.23	1.88	1.91	2.51	2.57

430 m × 220 m (796589 cells), and when the wind angle was 315°, the domain dimensions were 430 m × 420 m (872045 cells)…etc. However, the domain height was 82 m for all cases.

3.4. Wind tunnel experiments

Since the exceedance probability is calculated based on CFD simulations, it is very important to demonstrate that the numerical results are accurate. Wind tunnel experiments were carried out to validate the calculated flow fields through measuring wind velocity and pollutant concentrations. These experiments were performed in the boundary layer wind tunnel of the University of Tokyo.

In such experiments, the building patterns were represented by 1:100 scale wooden models and wind velocity and tracer gas concentrations were measured along the two sides of the street over an extended range of incident wind directions. Six directions have been considered and applied to each model. These directions were: 0°, 22.5°, 45°, 90°, 270°, and 315°. In each case, wind velocities and tracer gas concentrations were recorded along the two sides of the street at 1.5 m height.

Measurements of inlet wind velocity and turbulent intensity of the incident flow is performed using a 1-D hot wire probe constant temperature anemometer (CTA, Dantec®) using a frequency of 1.0 kHz with a sampling time of 65 s at each measurement location. To normalize the measured velocities, the reference velocity is set to be the velocity at roof level above the wind tunnel floor level in the free stream. For wind velocity measurements, a reference velocity of 4.6 m/s is considered; while for gas concentration measurements, a velocity of 0.78 m/s is applied.

Wind velocities at the desired locations are measured using thermal-type purified Germanium probes (GeZ-200M, Tohnic®). A total of 22 positions along the sides of the street at 1.5 m height are considered to perform the measurements, where a multi-channel anemo-thermometer system is used to measure the wind velocity at these locations simultaneously.

Measurements of pollutant concentrations are performed with a high response Flame Ionization Detector (FID) (THC-2A, TECHNICA®) equipped with a sampling needle. A mixture of ethylene (C_2H_4) and synthetic air is used as a tracer gas (ethylene is essentially neutrally buoyant in air). The concentration of C_2H_4 in the tracer gas is 12,100 ppm. A data acquisition system (NR-2000, KEYENCE®) along with a PC are used to record the concentration data. The locations where concentration measurements are taken are the same as those of the wind velocity measurements. For more details about the experiments, see Ref. [1].

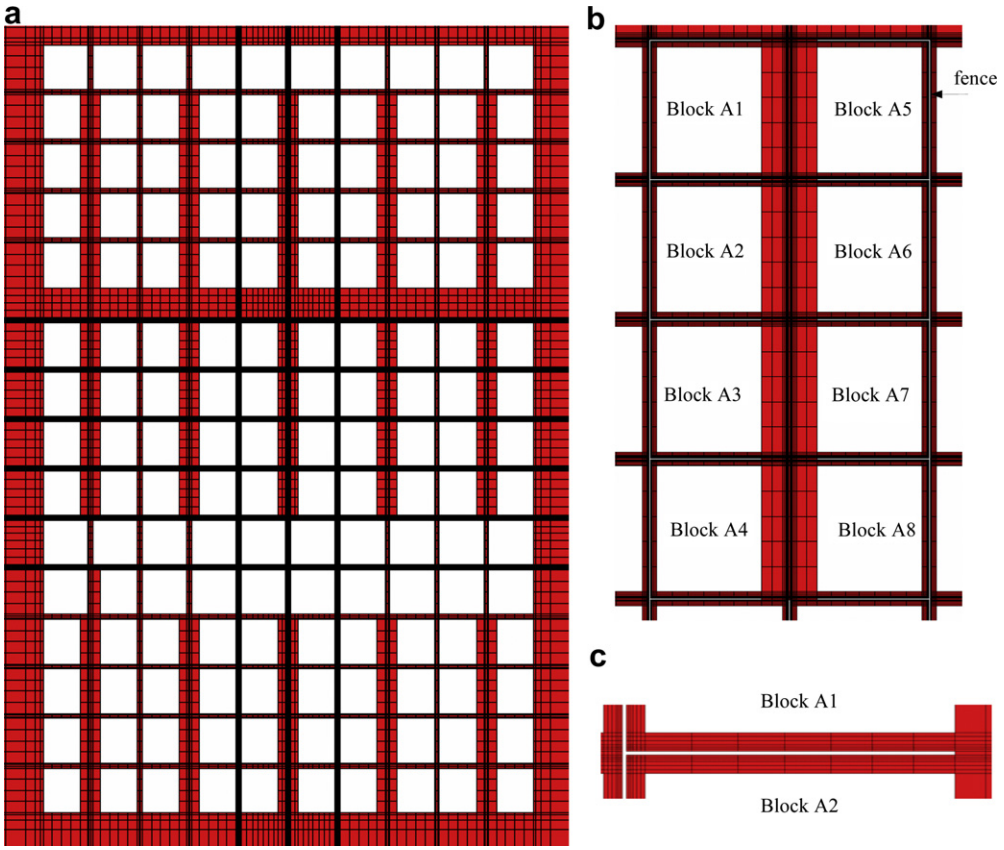

Fig. 6. Schematic representation of grid system to simulate the array of model (I); (a) grid system of the whole array; (b) grid system of the study domain; (c) grid system of the narrow passages between buildings.

Table 2
CFD simulation parameters together with applied boundary conditions.

Turbulent Model	The cubic k-ε model
Differential schemes	MARS [18] Diffusion term: Central difference scheme
Inflow conditions	$u = u_0\,(z/h)^{0.25}$, $u_0 = 1$ m/s & $h_0 = 74.6$ m $k = 1.5\,(u_0 \times I)^2$, $I = 0.10$ $\varepsilon = C_\mu^{1/2} \times k \times \frac{\partial u}{\partial z}$, $C_\mu = 0.09$
Outflow conditions	Zero normal derivatives
Side and top boundaries	Free slip
Building walls and ground	Generalized logarithmic law ($E = 9$)

4. Results and discussion

4.1. Comparison between numerical and experimental results

Some examples for comparing CFD simulation results with the experimental data for wind velocity at three levels of $z = 1.5$ m, 3.0 m and 9.0 m are presented in Figs. 7–9. Fig. 7 (a) shows the wind velocity in the region $y = 0$–40 m along the two sides of the street of model (I) at 1 m apart from the street center line. In the subplot (a), the calculated and the measured scalar velocities along the left hand side of the street ($x = -1$ m) at the three considered heights is shown. In numerical and experimental approaches, a general observation can be noticed that the velocity tends to increase from the inner end of the street ($y = 0$ m) to its open end ($y = 40$ m), which is located alongside the traffic road. Also, the figure shows satisfactory agreements between the numerical and experimental results along the inner half of the street ($0 \le y \le 20$) at $z = 1.5$ m and $z = 3.0$ m. However, a considerable difference is observed along the second half of the street ($20 < y \le 40$). These differences could be attributed to the fact that the measurement points near the traffic road ($y = 40$ m) are in locations of highly complex circulatory flow regions. In the same time, there are peak values for the wind velocity along this side of the street for these two wind directions near the narrow spaces between the street buildings. This behavior reflects the importance of the presence of such spaces between adjacent buildings to induce more wind through urban domains. Fig. 7(b) shows the wind velocities along the right hand side of the street ($x = 1$ m). Similar to the case of $x = -1$ m, good agreements are observed along the inner half of the street, while near the road side the differences between the two approaches are larger than those of the case of ($x = -1$ m). In Fig. 7 (a) and (b), at $z = 9$ m, a large difference between the calculated and the measured velocities are shown. The velocities calculated by CFD simulation underestimate the measured velocities. This can be attributed to the shortage of the turbulence model in predicting the velocity gradient near building walls and roofs.

In Figs. 8 and 9, the similar comparisons of numerical predictions with the experimental results for models (II) and (III) in the two wind directions are shown, respectively. Similar to the results of model (I), the numerical predictions of the two models, overall, are in satisfactory agreement with the experimental results, but the major discrepancies are present at $z = 9.0$ m. In addition to the shortages of the k-ε model in predicting the velocity gradient near walls and roofs, the computational errors include the inaccuracies introduced by the discretization scheme, parameter selection, and algebraic equation solutions. In general, however, the overall agreement between numerical predictions and experimental measurements is good.

4.2. Average wind kinetic energy within the study domain

Fig. 10 shows the average wind kinetic energy within the pedestrian domain of the street for the three building patterns versus the applied wind direction. Such quantities were estimated at a reference wind velocity of 1 m/s measured at a reference height of 74.6 m. The results demonstrate a significant dependence of the calculated wind kinetic energy on the incident wind direction and also on the building array geometry.

At almost all directions, models (I) demonstrate the lowest kinetic energy values compared with the other models. Such behavior reflects the high ventilation rate of model (I), which is attributed to the presence of narrow gaps between street buildings. The narrow gaps induce more wind to the street domain, which improves the ventilation process. Also, the effect of these gaps clearly appears in the case of model (III), which demonstrates low kinetic energy values compared with model (II), which has the highest average *KE* values among the three models at almost all wind directions. It is thought that the geometry of the solid U-shape in model (II) and the outer U-shape of model (III) are the main reasons for these trends. The U-shaped geometry prevents the wind from leaving the domain and forces the flow to generate vortices. This leads to increase the average wind *KE* within the domain.

In the range from $\theta_i = 180°$–$360°$, models (II) and (III) clearly demonstrate high *KE* values. The effect of wind direction in such range can be understood by realizing that most of the wind which enters the street domain comes through the shear layer at building roof level, while a low percentage of wind enters the domain through the traffic road side and the narrow gaps between street buildings. The wind flow through the narrow gaps creates lateral flows, which appear clearly in model (I) compared with model (III), while these flows disappear completely in the case of model (II). The interaction between these flows and the main flow coming

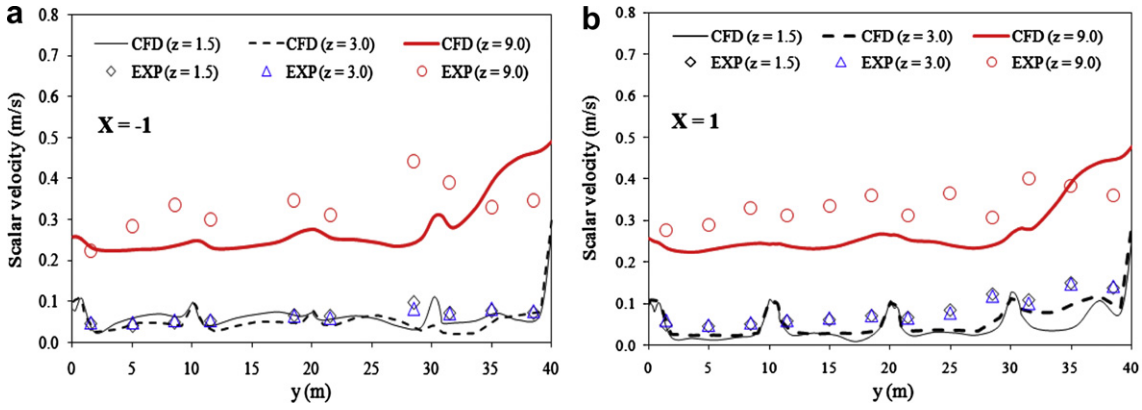

Fig. 7. Comparison between numerical and experimental wind velocities along the sides of the street of model (I) at $\theta = 0°$; (a) $x = -1$ m, and (b) $x = 1$ m.

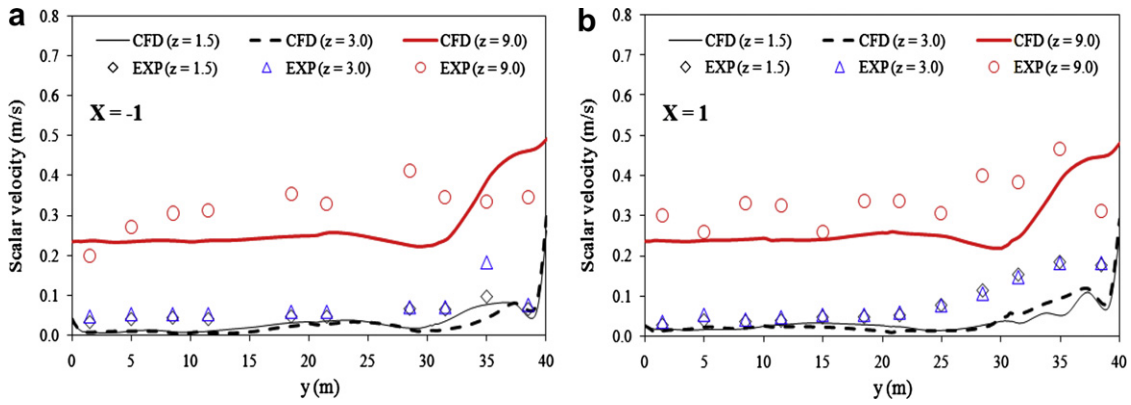

Fig. 8. Comparison between numerical and experimental wind velocities along the sides of the street of model (II) at $\theta = 0°$; (a) $x = -1$ m, and (b) $x = 1$ m.

across the shear layer creates a number of vertices within the street, which affect the *KE* of the main flow.

4.3. Application of exceedance probability

Results of calculating the total exceedance probabilities within the study domain for the three models are presented in Fig. 11. Each curve represents the total exceedance probability for the considered direction of the array. For example, the curve of NW-direction represents the total exceedance probability from the sixteen wind directions when the array direction is NW.

In Fig. 11, low probabilities are detected at high kinetic-energy values, while considerable probabilities are observed at low *KE* values. This can be attributed to the wind characteristics of Tokyo, reflected by the values of the parameters $C(a_n)$ and $K(a_n)$. As a general trend, the probability curves show a little divergence between the probabilities of the sixteen wind directions.

The figure demonstrates the low dependence of model (I) on the array direction compared with the other two models. This appears clearly in the convergence between the probability curves in the sixteen directions of the array. This means that the change in *KE* is very small with changes in the array direction in these kinds of densely urban areas.

From Fig. 11, it is clear that it will be difficult to evaluate the calculated exceedance probability for all of the sixteen directions due to the high density of the curves. So, it was preferred to compare the ventilation performance of the three building models based on the values of the average wind kinetic energy, estimated at the minimum probabilities. The minimum exceedance probabilities reflect low comfort conditions for inhabitants of these areas, which is important to be investigated.

4.3.1. Assessment of wind conditions based on KE

Fig. 12 shows the exceedance probabilities of the three building patterns, based on the average wind *KE* within the study domain. The sixteen model directions -starting from N to NNW in a clockwise rotation are signed with numbers from 0 to 15 and used as the horizontal axis in such figure. The average wind *KE* was considered as the key parameter and it is changed from 0.025 to 0.150 m^2/s^2 with a step of 0.025 m^2/s^2. The limited number for the values of *KE* is considered here since it is impossible to show the whole range on the same graph.

The figure shows that; the probability curves are almost symmetrical around the N-direction (SSE direction no. 7). This can be referred to the geometry of the building patterns. Also, the figure shows that; the maximum probability value is about 75%, and it is achieved by model (II), where model (II) shows the highest probability values among the three models for almost all wind directions. Another important note is that; the variation of the probability with the model direction becomes large as the *KE* value increases, where the significant difference between the maximum and the minimum probabilities are occurred at $KE = 0.10\ m^2/s^2$.

4.3.1.1. Influence of building geometry on exceedance probability. In order to investigate the influence of the different array geometries on the exceedance probability within the study domain, a certain values of *KE* is focused here. Such value has to reflect great variation in wind flow characteristics. Accordingly, the value of $KE = 0.10\ m^2/s^2$ is focused here. Fig. 13 shows the maximum and the minimum exceedance probability trends estimated at a kinetic energy value of 0.10 m^2/s^2. Also, the figure shows the directions at which these probabilities were calculated.

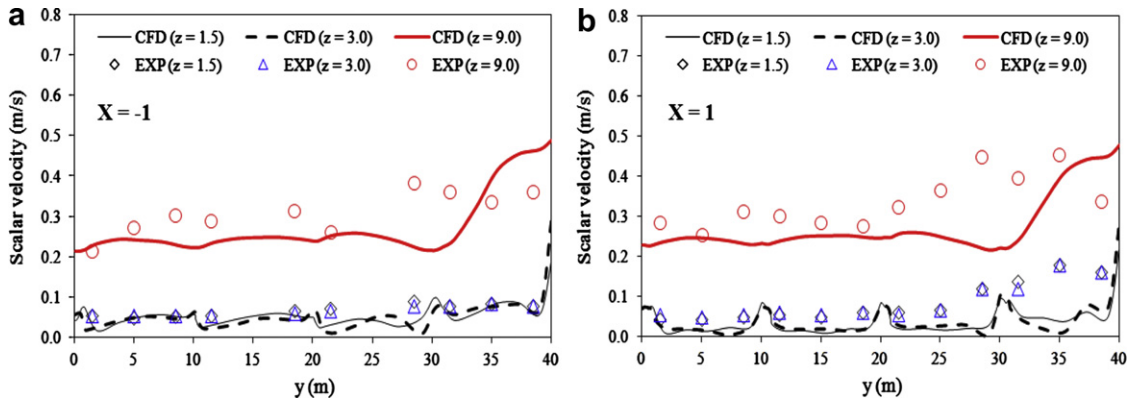

Fig. 9. Comparison between numerical and experimental wind velocities along the sides of the street of model (III) at $\theta = 0°$; (a) $x = -1$ m, and (b) $x = 1$ m.

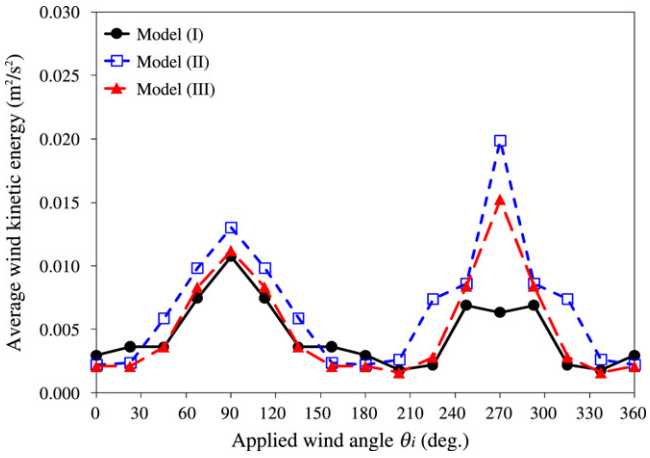

Fig. 10. Average wind kinetic energy within the study domain for the three patterns ($u_o = 1$ m/s).

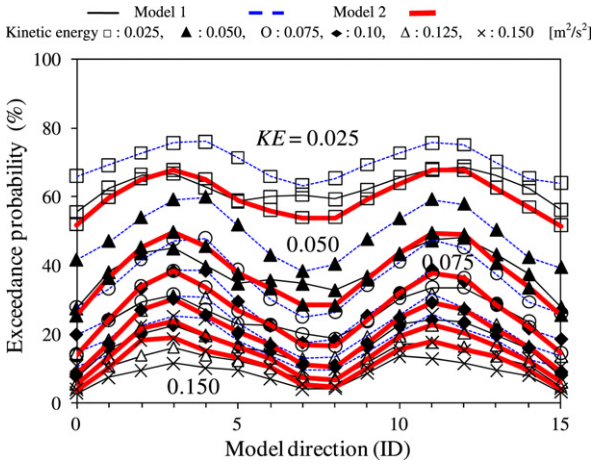

Fig. 12. Exceedance probabilities within the domain for the three building models.

In such figure, at low KE values (in the range of $KE = 0.05–0.2$ 2 m^2/s^2), the difference between the maximum and the minimum probabilities of model (I) is similar to that of models (II), while it is bigger in the case of model (III). On the other hand, at *KE* values greater than 0.2 m^2/s^2, the difference between the maximum and the minimum probabilities of model (I) (difference between □ and ■) is small, while such difference becomes large in the cases of models (II) (difference between △ and ▲) and (III) (difference between ○ and •). Referring to Fig. 5, the wind rose of Tokyo has two peaks at NNW and SW. This means the sensitivity of the probability to wind direction is high. In addition, the slope of the probability trends is large. This is attributed to the distribution of the Weibull parameter C_n, which has the same units of velocity according to Equation (3). The greater the value of C_n, the smaller the slope of the probability trends (and vice versa).

From the above discussion, it is clear that; when the wind characteristics in a certain area are investigated, the area wind rose is very important. It reflects the behavior of the incident wind for a certain direction of the building array. This means that; Fig. 5 together with Fig. 13, are important to study the wind characteristics in built-up areas.

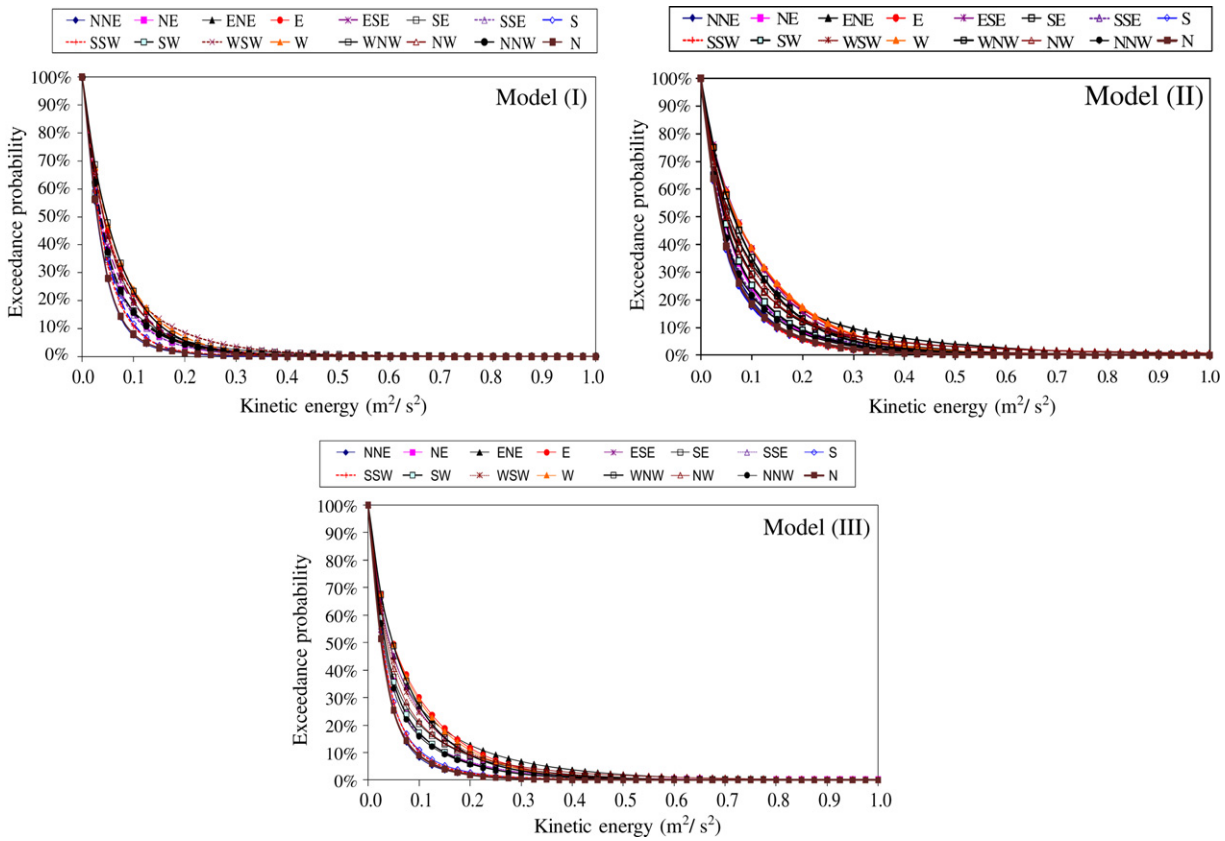

Fig. 11. Exceedance probability curves of the three models.

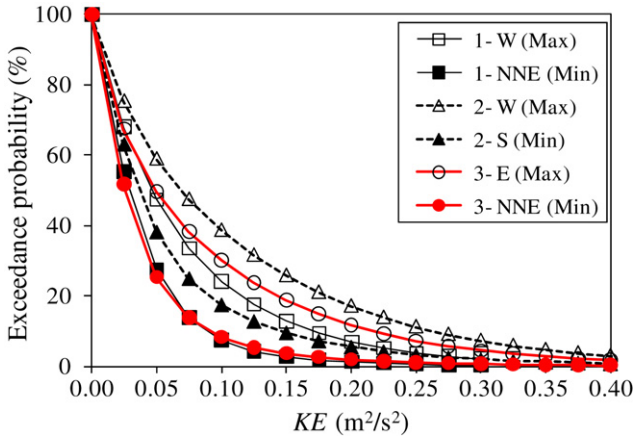

Fig. 13. Maximum and minimum 0.10 m^2/s^2 wind kinetic energy- based exceedance probability for the three models together with models directions of each case.

Table 3
Average wind *KE* values at the exceedance probabilities of 15% and 85% together with models directions.

Model (I)		Model (II)		Model (III)	
$P = 85\%$	$P = 15\%$	$P = 85\%$	$P = 15\%$	$P = 85\%$	$P = 15\%$
0.01169	0.10855	0.01557	0.18399	0.01158	0.12684
W	W	ESE	W	W	E

4.3.1.2. Assessment based on 85% and 15% exceedance probabilities. In order to assess the wind conditions of the three building patterns based on the calculated exceedance probabilities, a reasonable measure is required. Such measure should exhibit a time relevance of a repeating nature. Accordingly, it is adopted here to use the wind occurrence of a week as a base of comparison. One day per week reflects a probability of occurrence of 15% ($1/7 = 0.1428 \approx 15\%$) and six days per week reflect a probability of occurrence of 85% ($6/7 = 0.857 \approx 85\%$). So, the investigation of *KE* values at these two probabilities will be informative.

Table 3 presents the wind kinetic energy values for the three building patterns, at the two probabilities $P = 85\%$ and 15% together with models directions. According to the data given in the table, it is expected that the wind kinetic energy within the pedestrian domain of model (I) will be more than 0.011 m^2/s^2 for six days/week, and more than 0.108 m^2/s^2 for just one day/week. In model (II), these values are: 0.015 m^2/s^2 for six days/week, and more than 0.183 m^2/s^2 for one day/week. With respect to model (III), these values are: 0.011 m^2/s^2 for six days/week, and more than 0.126 m^2/s^2 for one day/week.

By comparing the *KE* values of the three building patterns, it is clear that; model (II) shows the highest probability values among the three models. However, since the minimum standard values of the wind kinetic energy for Tokyo is not exactly determined in the present stage of this study, it is difficult to state that model (II) is unacceptable.

5. Conclusions

Three typical models of a dense urban area were studied and numerically simulated to examine the effects of the geometry of these building patterns on wind flow characteristics within the pedestrian domain of a street located within this area. The exceedance probability was considered to assess the performance of the wind environment of the three models. A new approach for calculating the exceedance probability was introduced based on the average wind kinetic energy within the study domain as a reflection of comfort. The study was applied to Tokyo, based on its mean wind velocity data. The study revealed the following:

1) The exceedance probability seems to be an effective tool for evaluating wind conditions within urban domains.
2) The exceedance probabilities strongly depend on the geometries of the building arrays as well as the wind conditions of the construction site.

References

[1] Bady M, Kato S, Ishida Y, Huang H, Takahashi T. Exceedance probability as a tool to evaluate the wind Environment within densely urban areas. Wind and Structure November 2008;11(6).
[2] Blocken B, Carmeliet J. Pedestrian wind conditions at outdoor platforms in a high-rise apartment building: generic sub-configuration validation, wind comfort assessment and uncertainty issues. Wind and Structures 2008;11(1):51–70.
[3] Blocken B, Roels S, Carmeliet J. Modification of pedestrian wind comfort in the Silvertop tower passages by an automatic control system. Journal of Wind Engineering and Industrial Aerodynamics 2004;92:849–73.
[4] Blocken B, Stathopoulos T, Carmeliet J. Towards grid resolution guidelines for CFD simulations of wind speed in passages between buildings. In: The Fourth International Symposium on computational wind Engineering (CWE2006); 2006. p. 117–20 [Yokohama, Japan].
[5] Katsumata W. Strategies for improving the residential environment of existing suburban small-lot residential areas through harmoniously controlling the rebuilding of houses. PhD Thesis. The University of Tokyo, Japan (in Japanese).
[6] Melbourne W. Criteria for environmental wind conditions. Journal of Industrial Aerodynamics 1978;3(2–3):241–9.
[7] Melbourne W. Wind environment studies in Australia. Journal of Industrial Aerodynamics 1978;3(2–3):201–14.
[8] Mochida A, Tominaga Y, Murakami S, Yoshie R, Ishihara T, Ooka R. Comparison of various k-epsilon models and DSM applied to flow around a high-rise building- report on AIJ cooperative project for CFD prediction of wind environment. Wind and Structures 2002;5(2–4):227–44.
[9] Murakami S. Turbulence characteristics of wind flow at ground level in built-up area. Journal of Industrial Aerodynamics 1983;15:133–44.
[10] Murakami S. Study on acceptable criteria for assessing wind environment at ground level based on residents' diaries. Journal of Wind Engineering and Industrial Aerodynamics 1986;24(1):1–18.
[11] Murakami S, Mochida A, Hayashi Y. Modification of production terms in k-ε model to remove overestimate of *k* value around windward corner. In: The tenth wind engineering symposium of Japan; 1988. p. 199–201 [in Japanese].
[12] Ohba S, Kobayashi N, Murakami S. Study on the assessment of environmental wind conditions at ground level in a built-up area-based on long-term measurements using portable 3-cup anemometers. Journal of Wind Engineering and Industrial Aerodynamics 1998;28(1–3):129–38.
[13] Patankar S. Numerical heat transfer and fluid flow. New York: Hemisphere Publishing Corporation; 1980.
[14] Ratcliff M, Peterka J. Comparison of pedestrian wind acceptability criteria. Journal of Wind Engineering and Industrial Aerodynamics 1990;36(1–3):791–800.
[15] STAR-CD, Methodology, STAR-CD, version 3.22. Computational Dynamics Limited; 2004.
[16] Stathopoulos T. Pedestrian level winds and outdoor human comfort. Journal of Wind Engineering and Industrial Aerodynamics 2006;94:769–80.
[17] Tominage Y, Mochida A, Yoshie R, Kataoka H, Nozu T, Yoshikawa M, Shirasawa T. AIJ guidelines for practical applications of CFD to pedestrian wind environment around buildings. Journal of Wind Engineering and Industrial Aerodynamics 2008;96:1749–61.
[18] Visser G, Cleijne J. Wind comfort predictions by wind tunnel tests: comparison with full-scale data. Journal of Wind Engineering and Industrial Aerodynamics 1994;52:385–402.
[19] Wind Engineering Institute of Japan. Fundamentals of wind around buildings. Kajama Publisher; 2005.